Design, construction and evaluation of a new laboratory convective dryer using CFD

D. A. Tzempelikos, A. P. Vouros, A. V. Bardakas, A. E. Filios, and D. P. Margaris

Abstract—In order to overcome the lack of experimental data in the open literature and the necessity to validate numerical models, as well as increase the efficiency of the drying process, a new laboratory convective (LC) dryer has been designed, constructed and equipped with an integrated measurement and automated control instrumentation. The main sections of the LC dryer, which can be arranged for operation in a closed or open circuit mode through manually controlled dumpers, are the vertical flow drying chamber, the tube heat exchanger, the thermal boiler and finally the fan - motor with a smooth speed control unit. The experimental facility tested and monitored the moisture content removal of horticultural and agricultural products. The current paper outlines the methodology applied for the design and optimization of the LC dryer, which has been achieved through the analysis of the flow field by means of computational fluid dynamics (CFD). The prediction of the 3d flow problem was accomplished through the solution of the steady-state incompressible, Reynolds-Averaged Navier-Stokes (RANS) equations with the incorporation of the standard k-ε turbulence model. The measurement and control instrumentation with the inclusion of the innovative, pc-controlled, 3d traverse system that serves detailed surveys of the temperature and velocity inside the drying chamber, are also discussed. The performance test and evaluation of the LC dryer was conducted using quince slices as a test material at an average temperature of 60°C and air at 2 m/s into the drying chamber.

Keywords—CFD, Convective dryer, Design, Drying kinetics.

I. INTRODUCTION

ONE of the major objectives in the drying process is to achieve a uniform moisture content in the final product. The uniformity of the moisture in the final dried product may be achieved through the proper distribution and guidance of the drying air inside the drying chamber. The air distribution depends on the drying process, the product to be dried and the geometry of the drying unit. The above factors determine the uniformity of drying and the final product quality. The velocity distribution can be determined based on the conservation equations for mass and momentum. Analytical solutions can be found only in simple cases. The variables involved in the air flow can be determined experimentally, but it is a tedious, time consuming and costly process. Moreover, it can only be applied to in service units. Hence, it cannot be used to optimize the drying chamber at an early phase of the design. In cases of complex geometry the employment of computational fluid dynamics (CFD), is an efficient way to evaluate the quality of the airflow. The CFD technique is a very powerful tool with great applications in both industrial and non-industrial installations.

CFD has been used in several studies that focused on the design and optimization of drying process. Kiranoudis, Karathanos and Markatos [1] simulated an industrial batch-type, tray air dryer using the standard k-ε turbulence model. The simulated profile of the flow field, temperature and humidity of the air phase revealed a lack of spatial homogeneity of air conditions above the product. Roman, Stahl-Schafer and Hensel [2] improve the air distribution in a fixed-bed dryer using CFD. The modified version resulted in much more homogenous air distribution and drying rates. Margaris and Ghiaus [3] simulated the airflow in an industrial drier and provided parameters for a different configuration that helped to optimize the drying space with significant improvement in the quality of the dried product and the reduction of energy consumption. Amanlou and Zomordian [4] designed a new fruit cabinet with different geometries and simulated them using CFD. The experimental results and the predicted data from the CFD revealed a very good correlation coefficient for the drying air temperature and air velocity in the drying chamber. Mathioulakis, Karathanos and Belessiotis [5] simulated the flow of air in an industrial batch-type, tray air dryer. The distribution of pressure and velocity over the product were found to lack in spatial homogeneity which led to variations in the drying rates and moisture contents. Norton and Sun [6] in a review paper showed the wide use of CFD for predicting the air velocity and temperature in drying chambers.

The present effort involves the design, construction and evaluation of a new LC dryer which can be used for the drying

D. Tzempelikos is a PhD Student in the Fluid Mechanics Laboratory, Department of Mechanical Engineering and Aeronautics, University of Patras, GR-26500 Patras, GREECE (corresponding author, phone: +30-210-2896838; fax: +30-210-2896838; e-mail: dtzempelikos@meed-aspete.net).

A. Vouros is a PhD Researcher in the Laboratory of Fluid Mechanics and Turbomachinery, Department of Mechanical Engineering Educators, School of Pedagogical and Technological Education (ASPETE), GR-14121 Athens, GREECE (e-mail: avouros@meed-aspete.net).

A. Bardakas is an undergraduate student in the Laboratory of Fluid Mechanics and Turbomachinery, Department of Mechanical Engineering Educators, School of Pedagogical and Technological Education (ASPETE), GR-14121 Athens, GREECE (e-mail: abardakas@meed-aspete.net).

A. Filios is a Professor in the Laboratory of Fluid Mechanics and Turbomachinery, Department of Mechanical Engineering Educators, School of Pedagogical and Technological Education (ASPETE), GR-14121 Athens, GREECE (e-mail: aefilios@meed-aspete.net).

D. Margaris is an Associate Professor in the Fluid Mechanics Laboratory, Department of Mechanical Engineering and Aeronautics, University of Patras, GR-26500 Patras, GREECE (e-mail: margaris@mech.upatras.gr).

of organic and non-organic products through a complete automated control system. The flow field within the drying chamber was studied using the CFD commercial code Fluent®. For the numerical simulations the steady state RANS equations were solved in combination with the standard k-ε turbulence model. Aiming for an initial evaluation of the laboratory scale dryer, an experimental investigation of the drying kinetics of quince slices under predefined drying conditions (drying temperature 60°C and air velocity 2 m/s) was performed.

II. DESCRIPTION AND DESIGN ASPECTS OF THE LC DRYER

The LC dryer which has been designed, constructed and evaluated in the Laboratory of Fluid Mechanics and Turbomachinery in ASPETE is shown in Fig. 1 and 2. The overall dimensions of the facility plant are 4.7 m (length) x 2.5 m (width) x 2.5 m (height). The construction of the air ducts

unit while, with the adjustment of the air dampers, the laboratory dryer can be used for thermal drying experimental studies in both open circuit and close circuit operations.

A. Tube Heat Exchanger and Boiler

The design specifications of the LC dryer require a continuous operation of the dryer in open circuit mode with an airflow velocity of 3 m/s and a temperature of 80°C into the drying chamber. The selected tube heat exchanger, air – water, with a capacity of 45.94 Gcal/h and overall dimensions of 630 mm (length), 200 mm (width) and 550mm (height) serves the required specifications. The tube heat exchanger consists of twenty circuits with six tubes per circuit (diameter 3/8 in of each tube) and a collector of 1 and ¼ in. The distance between the fins is 2.3 mm.

A standalone system boiler with a thermal power of 58 kW (50 Gcal/h) covers the requirements of the installed tube heat exchanger. The water pump meets the specifications of the

(1) Fresh air inlet
(2) Inlet damper
(3) By pass air damper
(4) Outlet damper
(5) Air outlet
(6) Centrifugal fan
(7) Three-phase electric motor regulated by an AC inverter
(8) Diffuser
(9) Temperature and humidity sensors
(10) Tube heat exchanger
(11) Guide vanes
(12) Metal frame for pressure cells
(13) Flow straighteners
(14) Temperature and humidity sensors
(15) Load cells
(16) Metal tray
(17) Temperature and humidity sensors
(18) PC controlled 3-axis traverse system
(19) Drying chamber
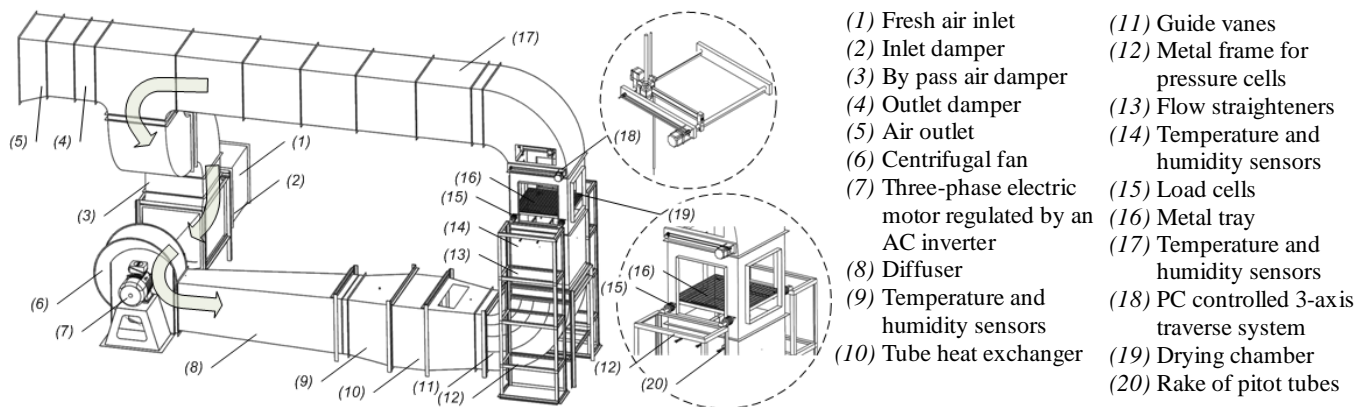(20) Rake of pitot tubes

Fig. 1 Schematic diagram of the LC dryer (curved arrows show the flow direction when dryer is in closed circuit operation)

was galvanized steel of 0.8 mm thickness. All the ducts are thermally insulated with 10 mm Alveolen (Frelen) with thermal conductivity of 0.032 W/mK.

The LC dryer downstream of the centrifugal fan outlet consists of a long rectangular diffuser with 6.7° total divergence angle that combines an optimum diffusion angle which minimizes losses [7], a tube heat exchanger that provides the required thermal power to the air stream, a transitional duct with observation window that includes the sprayer for humidifying purposes, a corner duct that incorporates three guide vanes (Fig. 3), a flow straightener section in order to achieve flow uniformity in the drying section, a drying chamber with a metal tray (Fig. 4) and the computer controlled 3-axis traverse system (Fig. 5 & 6), a second corner duct with guide vanes, an elevated horizontal modular constructed duct, an outlet dumper and an exit diffuser.

The modular design of the facility permits the easy placement of two or three horizontal drying chambers in tandem arrangement, on the elevated return or exit flow leg. The flow rate is observed and controlled with a custom made and calibrated rake of pitot tubes, located at the inlet of the drying chamber (Fig. 7).

The air flow is established and controlled through the drive

Fig. 2 Photo of the LC dryer, equipped with measuring instrumentation and data acquisition system

heat exchanger. The operations of the boiler and the water pump are controlled through custom application developed in Labview® software development environment.

B. Air and Humidity Spray Nozzle

To maintain the air humidity in the drying chamber at a

constant required level, a water supply system was designed, constructed and placed downstream of the tube heat exchanger. The system consists of a brass nozzle with two inputs, one for water and one for air.

For air supply, an air compressor with tank volume of 24 lt and 8 bar pressure, as well as a system of three filters of different classification levels for its purity, are used. For the water supply, the water system of the laboratory with the necessary filters is utilized. Two solenoid valves regulate the operation of the fresh air and humidity nozzle system.

C. Air Stream Guidance Devices

The air stream guidance devices are those that assist the flow a) to follow the curvature of the 90-deg corners upstream and downstream of the drying chamber with small loss and b) to reduce lateral variations in average velocity prior to its entrance in the drying chamber [8, 9].
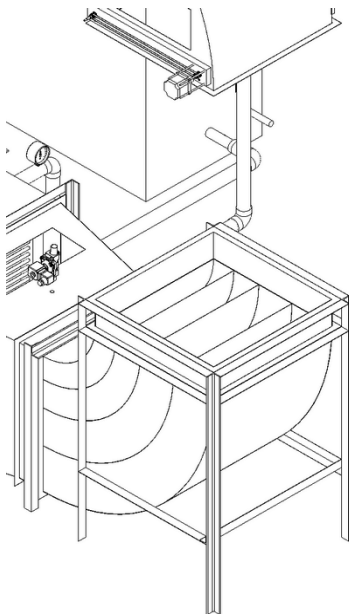

Fig. 3 Upstream corner with guide vanes

The design of the guide vanes in the 90-deg corners is based on potential flow calculations. Each guide vane section consists of three guide vanes unequally spaced, as shown in Fig. 3. The distances between the guide vanes are 86.6 mm, 105 mm and 140 mm respectively.

The flow straightener placed upstream of the drying chamber consists of an aluminum hexagonal honeycomb with a thickness of 38 mm, a cell size of 6.35 mm and a ratio (length to diameter) of about 6 (Fig. 1). The permeability of the honeycomb is 84.24%, while its resistance coefficient is 0.20 [10]. The outlet face of the honeycomb is partially covered with coarse mesh screens distributed and fixed in place following the preliminary calibration of the drying chamber.

D. Drying Chamber and its Instrumentation

The square section drying chamber is of tower (vertical) type and its dimensions are 0.5 m x 0.5 m x 0.66 m. A set of four refractory glasses of 10 mm thickness are available to replace the side steel walls when optical clarity and precise

visual observations are required. Pressure taps and probe insertion holes are provided for serving the experimental surveys. The drying chamber of the LC dryer is equipped with a metal tray, a rake of pitot tubes placed in a fixed position downstream of the honeycomb and a PC controlled 3-axis traverse system, all of which are considered as the standard instrumentation of the drying chamber.

The metal tray is located inside the drying chamber in a distance of 0.295 m from the inlet and is supported on four load cells mounted on an external base (Fig. 4). The tray has a length of 0.40 m, width of 0.44 m and thickness of 2.98 mm. The dimensions of the orthogonal holes are 23.94 mm x 11.29 mm. A gap of 10 mm along and 6 mm widthwise exists between the tray and the walls of the drying chamber. The permeability is 78.32%, while the resistance coefficient is 0.452 [11, 12].

A 3-axis computer controlled traverse (CCT-3A) with probe holder has been designed, constructed and tested, aiming to
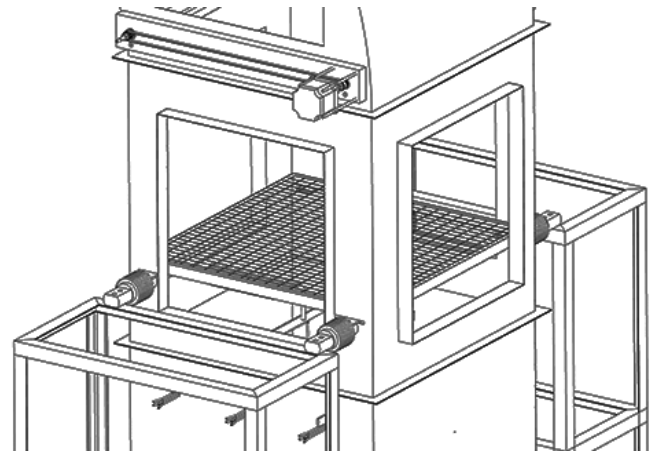

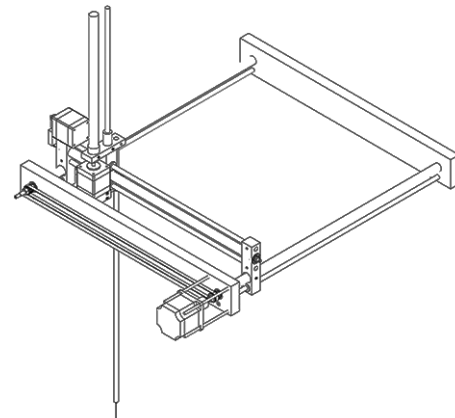Fig. 4 Drying chamber with the metal tray on load cells

Fig. 5 Detailed view of the CCT-3A

serve flow field surveys into the drying chamber. The x-y-z traversing system mounted at the end of the drying chamber is capable to traverse a probe (hotwire, temperature, pressure) in space with dimensions 380 mm x 480 mm x 200 mm. The position accuracy on each axis is 0.1mm, the resolution of each axis is 0.05 mm, the operating temperature is -10 to 70°C and the maximum power consumption is 48 Watt. The driving power is provided by a lead screw – nut assembly

coupled with a bipolar stepper motor (open-loop) for each direction/axis. Each axis slides on a linear bearing – shaft configuration for reduced friction. The control of the 3-axis traverse is achieved by an electronic unit with USB connectivity and the application for driving the traverse is developed in Labview® software development environment.
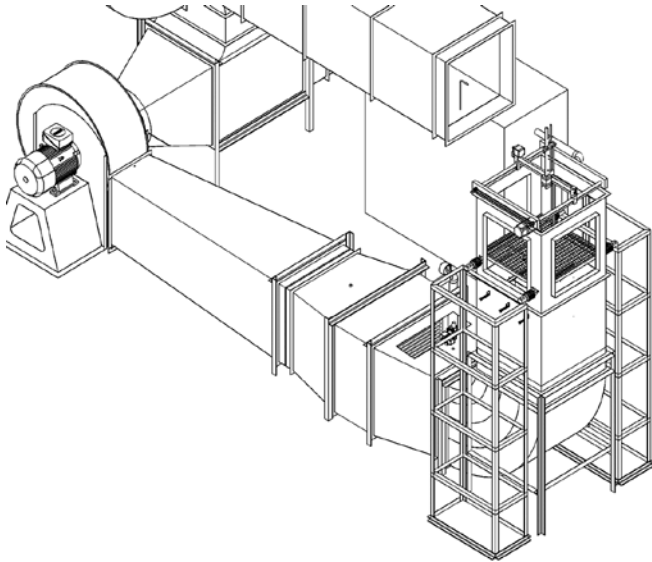
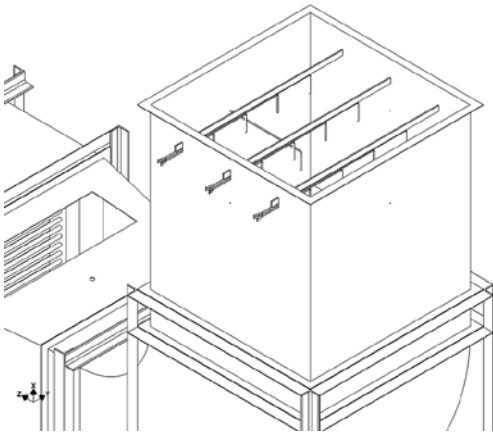

Fig. 6 Position of the CCT-3A in the LC dryer

Fig. 7 Rake of pitot tubes

The mean speed of the air flow at the inlet is the weighted average velocity of the 12 points collected from the rake of pitot tubes as shown in Fig. 7 and the four pressure taps located on the side walls. Each pitot tube is connected via plastic tubing to a custom made pressure collector system equipped with solenoid valves that are PC-controlled. All pitot tubes were calibrated against a velocity reference transducer which is the best balance between cost and accuracy. The velocity range of the sensor is 0 – 30 m/s. The calibrated accuracy is ±2% of reading ±0.02 m/s, which is assured by a certificate provided by the manufacturer.

E. Drive Unit and Pressure Losses

The drive unit consists of a single inlet centrifugal fan designed for the continuous extraction of air stream up to 80°C. The impeller of the fan is of backward curved blades design and it is manufactured from electro-welded sheet metal

protected against corrosion by an epoxy-polyester paint coating. The fan is driven directly by a 3 phase electric motor of 3 kW with its speed regulated by an AC inverter. The AC inverter is controlled using the RS-485 protocol with a USB connectivity converter. Custom application in Labview® software development environment controls the operation of the drive unit, providing a remote access option.

The energy provided by the centrifugal fan compensates the energy losses which occur in each section of the LC dryer with the latter depending on the local dynamic pressure and the local loss coefficient. The total pressure losses in the LC dryer are calculated by:

$$\Delta p_{tot} = \zeta_{tot} \frac{1}{2} \rho u_{avg}^2 \tag{1}$$

where Δp_{tot} is the total pressure loss (Pa), ζ_{tot} is the total loss coefficient based on the drying chamber dynamic pressure, ρ is the drying air density (kg/m^3) and u_{avg} is the drying chamber mean velocity (m/s). It is difficult to predict from theoretical calculations what these losses will be so they are almost always determined from experimental data. Idelchick [13] has made a thorough examination of all the parameters that affect these losses. A value of 43 has been calculated for the total loss coefficient for the LC dryer.

III. Numerical Simulations

The flow field predictions in the LC dryer were obtained using the Fluent® steady RANS solver following the discretization in space by a structured grid (3x10^5 nodes), utilizing a Gambit® preprocessor. The grid was refined close to the walls, in between the wall and the tray and inside the tray. The y$^+$ was in the range of 30 to 50. The grid independence was checked and a converged solution was obtained after approximately 500 iterations.

The Reynolds averaged equations were complemented by two additional convection diffusion-reaction equations for the computation of the turbulent kinetic energy and dissipation rate according to the standard k-ε turbulence model [14]. The standard logarithmic wall functions were applied to bridge the viscosity affected region between the wall and the fully turbulent region. The SIMPLE algorithm was used for the solution of the pressure-velocity coupling equations. The second-order-upwind scheme was chosen to improve numerical accuracy.

A source term was added to the k-ε turbulence model equations for the estimation of the pressure drop across the dryer. The heat exchanger, the honeycomb and the metal tray were modeled as a thin porous media of finite thickness over which the pressure changes are defined as a combination of Darcy's law and an additional inertial loss term and are given by [15]:

$$\Delta p = -\left(\frac{\mu}{\alpha} U + C_2 \frac{1}{2} \rho U^2 \right) \Delta m \tag{2}$$

where μ is the laminar fluid viscosity, α is the permeability of the medium, C_2 is the pressure-jump coefficient, U is the velocity normal to the porous face and Δm is the thickness of the medium.

The inlet boundary condition was set at a constant velocity of 4 m/s normal to the inlet boundary. The turbulent intensity, which is defined as the ratio of the root-mean-square of the velocity fluctuations, to the mean flow velocity, was set at 3.95% with the value derived from the following empirical formula [15]:

$$I = \frac{u'}{u_{avg}} = 0.16\left(\mathrm{Re}_{D_h}\right)^{-1/8} \tag{3}$$

where D_h is the hydraulic diameter of the duct.

The atmospheric pressure boundary located downstream of the outlet duct was specified as the pressure outlet. The no slip boundary condition was used in all the walls.

For the numerical simulations, a desktop PC (Intel® Core i7 CPU at 2.67 GHz) was used. The number of iterations was adjusted to reduce the scaled residual below the value of 10^{-6} which is the criteria. For each run, the observation of the integrated quantities of total pressure, at suction as well as at discharge surface was appointed for the convergence of the solution. In many cases this drove the residuals to lower values than the initial set value. Depending on the case, the convergence was achieved at difference iterations, as the result of a specific mass-flow being used to initialize the computations at another mass-flow. Aiming to smooth convergence, various runs were attempted by varying the under-relaxations factors. In that way, a direct control regarding the update of the computed variables through iterations was achieved. Initializing with low values for the first iteration steps and observing the progress of the residuals, these values were modified aiming for the acceleration of the convergence.

IV. DRYING EXPERIMENTS

A. Materials

Fresh quinces were purchased from a local market in Athens, Greece and used in the drying experiments. The samples were stored in a refrigerator at about 6°C until use. Before drying, the quinces were cleaned and sliced manually to a thickness of 10 mm in order to produce uniform quince pieces. The samples were used to form a thin-layer on a 440 mm x 400 mm tray with a net weight of 395.5 gr. The initial moisture content (M_0) of quince slices was measured to be around 81.04% in wet basis (w.b.) or 4.27 kg water / kg dry matter in dry basis (d.b.) and was determined by the oven-drying method [16] repeatedly in order to assure accurate moisture content average values.

B. Experimental Procedure

The LC dryer was started 2h before each experiment in order to achieve the desired steady state conditions. Then the metal tray of the drying chamber was filled with about 700 gr

sliced quinces in thin-layer form. The experiments were performed at air drying conditions of 60°C with 4% relative humidity. The air velocity was adjusted to 2 m/s in the drying chamber. The volumetric flow rate was 1800 m³/h, corresponding to a Reynolds number of 7.3 x 10⁴.

Weight, air temperature, probe-surface temperature and relative humidity were automatically monitored and acquisitioned. Measurements were taken every 10 min. All experiments were twice repeated and the means of measurements were averaged and used to express the data of the moisture content.

C. Modeling of Drying Kinetics

The moisture content of the samples and the dimensionless moisture ratio (MR) during the drying processes were found by applying the following equations:

$$M_t = \frac{w_t - w_d}{w_d} \tag{4}$$

$$MR = \frac{M_t - M_{eq}}{M_0 - M_{eq}} \tag{5}$$

$$DR = \frac{M_{t+dt} - M_t}{dt} \tag{6}$$

where M_t is the moisture content at any given time t (kg water / kg dry matter), w_t is the dry matter at any given time t (kg), w_d is the dry matter (kg), M_0 and M_{eq} are the initial and equilibrium moisture content (kg water / kg dry matter) respectively, DR is the drying rate (gr water / h) and M_{t+dt} is the moisture content at $t + dt$ (kg water / kg dry matter).

M_{eq} is quite small compared to M_0 and M_t and in the MR definition it can be ignored [17]. The mass transfer equations during convective drying have been applied under the following assumptions: i) The process is isothermal, ii) the main transfer mechanism is diffusion and iii) the deformations and shrinkage during drying are negligible [18]. The experimental data was fitted by the Page [19] thin-layer drying model:

$$MR = \exp\left(-kt^n\right) \tag{7}$$

where the values for the drying constants k and n were used from [20].

D. Instrumentation and Data Acquisition

The air and drying product temperatures were measured using a calibrated PT100 with accuracy ±0.15°C. A 3-wire transmitter with accuracy ±0.2°C was used for the above PT100's.

The relative humidity of the drying air was determined using calibrated humidity transmitters with accuracy ±2.95 %. A differential pressure transmitter, with a calibrated accuracy ± 2% of the selected range of 25 Pa, was used to measure air drying velocity at the inlet of the drying chamber while inside

the drying chamber a 2-D hot wire anemometer was used.

The anemometer probe used in the LC dryer was a dual sensor (X-probes) miniature wire of 5 μm in diameter and 1.2 mm long, suspended between two needle shaped prongs for each sensor.
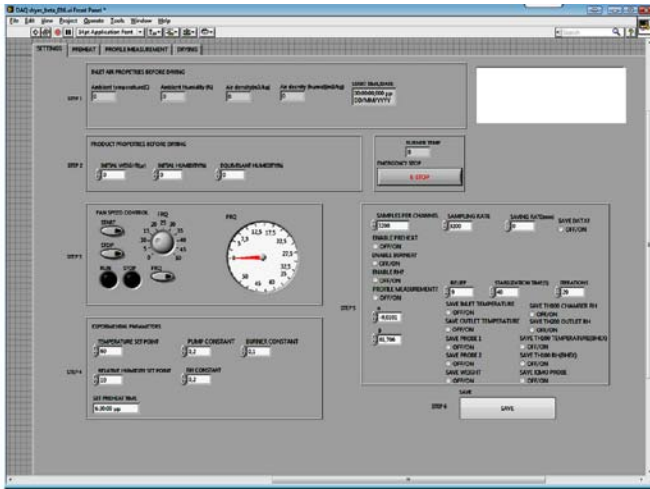

Fig. 8 Visual instrumentation of the LC dryer

The weight was quantified using four load cells (total nominal load 10 kg) with accuracy ±0.05% and an analog transmitter with accuracy ±0.03%.

All transmitters are connected to a PC with a PCIe-6321 DAQ device (National Instruments®) via NI SCXI-1000 and NI SCXI-1302 modules with accuracy ±0.134% and a sampling frequency of 3.2 kHz. Custom application in Labview® software development environment was used to interface with the data acquisition (Figure 8).

V. RESULTS AND DISCUSSION

A. Flow Simulations

The flow field in the empty LC dryer, operated in open circuit mode, was numerically analyzed. Two cases are presented in the current study. In the first case, the airflow simulations were performed in the absence of internal components into the ducts, i.e. heat exchanger, guide vanes, honeycomb and metal tray in the drying chamber. In the second case, the presence of the internal components was considered. In both airflow simulations, constant temperature (T = 60°C) was assumed in the flow volume.

The quality of the flow into the LC dryer is evaluated in terms of velocity and pressure variations into the drying chamber. The following non-dimensional parameters are used:

$$U_{var} = \frac{u_i - u_{avg}}{u_{avg}} \tag{8}$$

$$c_p = \frac{p_i - p_{inlet}}{(1/2)\rho u_{avg}^2} \tag{9}$$

where U_{var} is the dimensionless velocity variation, u_i is the velocity (m/s) at an ith position, u_{avg} is the mean flow velocity (m/s) at the inlet of the drying chamber, c_p is the non-dimensional pressure or pressure coefficient, p_i is the static pressure (Pa) at an ith position, p_{inlet} is the average static pressure (Pa) at the inlet of the drying chamber, and ρ is the drying air density (kg/m^3).

Fig. 9a and 9b show the flow pathlines for the two cases. At the outlet of the centrifugal fan the air velocity approaches 4 m/s and then normalizes to the design level of 2 m/s.

Fig. 10 illustrates U_{var} at certain positions in the drying chamber, namely at 415 mm and 535 mm from the inlet and 250 mm in depth, for both examined cases. In Fig.10a it is observed that 10 cm from the walls of the drying chamber, the U_{var} changes from -20 % to 20%. In particular, the U_{var} profile is higher to the right side of the chamber relatively to the left side. This is apparently due to the non-uniform flow from the 90° guide inlet corner to the drying chamber.

In Fig. 10b, the U_{var}, at the same distance from the walls of the drying chamber, remains almost zero. This is mainly due to the presence of the guide vanes in the 90 deg corners that contribute to a more uniform flowfield.
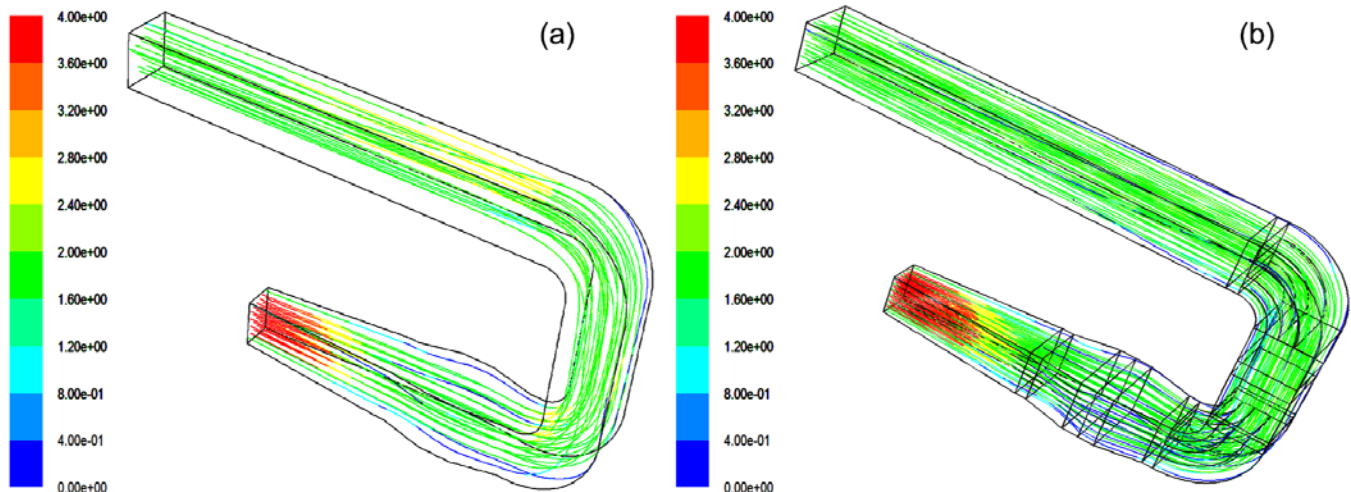

Fig. 9 Pathlines of air velocity magnitude; a) empty dryer and b) equipped dryer

Fig. 10 Dimensionless velocity distribution at z = 415 mm (Rake A) and z = 535 mm (Rake B)

Fig. 11 Contours of dimensionless velocity variation at z = 415 mm

Fig. 12 Dimensionless pressure coefficient distribution at z = 415 mm (Rake A) and z = 535 mm (Rake B)

The overall evaluation of the quality of the flow in the drying chamber can be deduced with the aid of Fig. 11. The iso-contours of U_{var} at a level of 415 mm from the inlet when the empty LC dryer is considered are shown in Fig 11a. The U_{var} varies up to 25% while in the same level, U_{var} varies up to 4% (Fig. 11b) when the internal components of the dryer are present.

Consequently, the heat exchanger, the guide vanes and the honeycomb, apart from their contribution to pressure losses, act positively in the improvement of the flow uniformity across the whole drying chamber.

The non-dimensional pressure variation across the drying chamber at two z-locations along the drying chamber is shown for both examined cases. In Fig. 12a, it is shown that c_p varies

from -0.18 to 0.21 while in Fig. 12b, c_p varies from -0.7 to -0.8.

In the latter case, the lower value of the c_p is apparently due to the fact that in case (b) the pressure losses are higher but the pressure gradients across the chamber are almost eliminated.

B. Drying Experiment

The curve of moisture ratio versus drying time is shown in Fig. 13a. It is observed that the MR decreases with time when stabilized after twelve hours of drying. Fig. 13b shows the

data mainly scatters adjacent to the 45° (perfect fit, X = Y) straight line within the upper and lower predictions limits, thus this model can represent the drying characteristics of the quinces accurately.

Fig. 14b shows the comparison between measurements and the Page thin-layer drying model, simulated at 60°C and 2 m/s. While slightly underestimating the MR in the final stage of the drying experiment there is a good agreement between the measurements and the prediction when using the Page model.
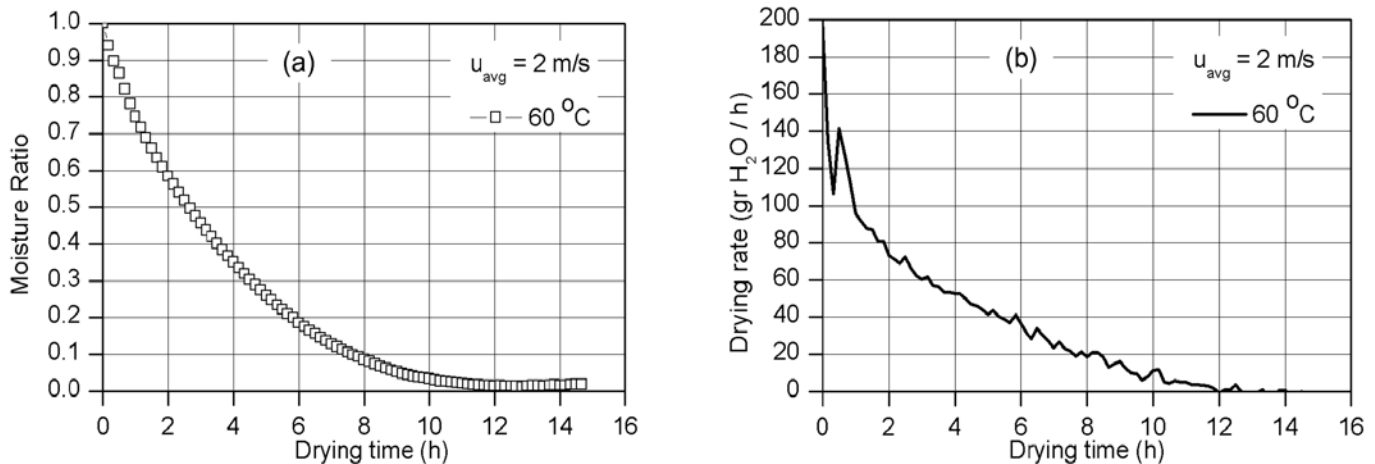

Fig. 13 (a) Moisture ratio versus drying time (b) Variation of drying rate as a function of drying time
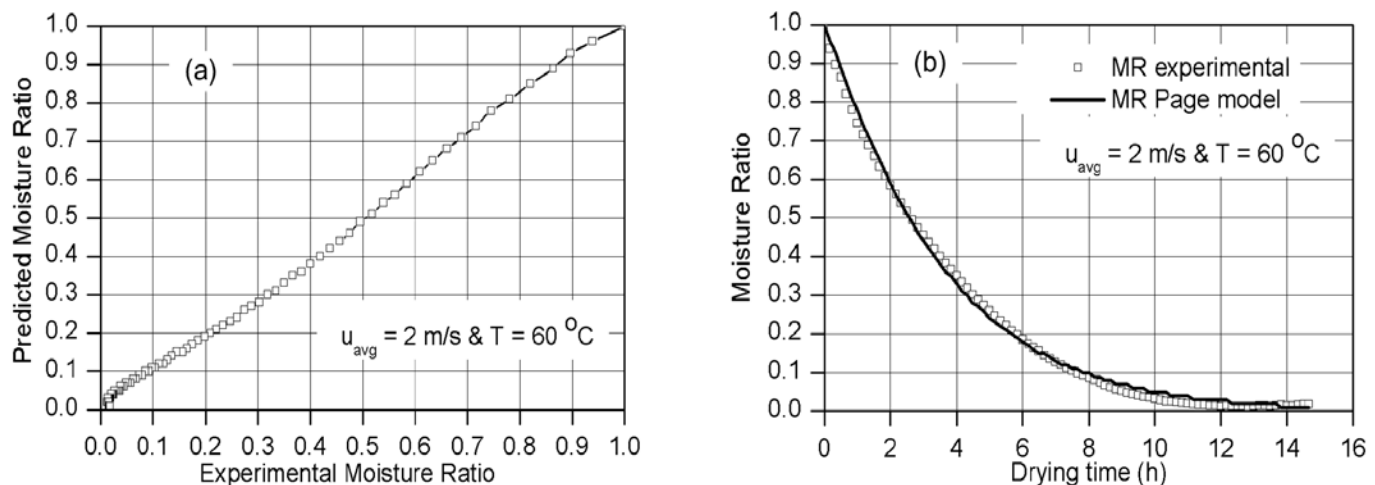

Fig. 14 (a) The experimental MR versus the MR predicted by Page model (b) Comparison of the selected model fitted for quince

change in drying rate as a function of drying time at the drying temperature of 60°C.

It is apparent that the drying rate decreases continuously with the drying time. A constant period was not detected in the drying experiment. Hence the entire drying process for quince slices occurs in the range of the falling rate period. This shows that diffusion is the dominant physical mechanism governing the moisture movement in the samples. Similar results were obtained by different authors [21-27] who dried various agricultural products.

The predicted MR of the Page thin-layer drying model compared to the experimental results is shown in Fig. 14a. The

VI. CONCLUSIONS

In this study, a fluid flow model of a new LC dryer, including its major features, is developed using the CFD code Fluent® as a tool to improve the performance of an LC dryer by improving the air distribution in the drying chamber.

The standard k-ε turbulence model was used for computing turbulence parameters inside the air dryer. It was seen that by use of three guide vanes at the 90° inlet corner, a much more uniform air distribution in the drying chamber could be achieved.

For the evaluation of the LC dryer, the drying kinetics of

the quince slices were studied as a function of the drying conditions. Experiments were carried out at 60°C and 2 m/s.

It was observed that the drying rate decreases continuously with drying time. A constant period was not detected in the drying experiments. Hence, the entire drying process for quince slices occurs in the range of the falling rate period.

In order to describe the drying behavior of the quince slices, the Page thin-layer drying model was fitted to the drying data, demonstrating fine agreement with the experimental results.

NOMENCLATURE

c_p	Non-dimensional pressure
C_2	Pressure jump coefficient (m^{-1})
DR	Drying rate (gr water / h)
I	Turbulent intensity (%)
k, n	Constants in Page thin-layer drying model
M_{eq}	Equilibrium moisture content (kg water / kg dry matter)
M_0	Initial moisture content (kg water / kg dry matter)
MR	Moisture ratio
M_t	Moisture content at any time moment t (kg water / kg dry matter)
M_{t+dt}	Moisture content at any time moment t+dt (kg water / kg dry matter)
Re	Reynolds number
T	Drying temperature (^{o}C)
U	Velocity normal to the porous face (m/s)
U_{var}	Dimensionless velocity variation
p	Pressure (Pa)
t	Drying time (h)
u	Velocity (m/s)
u'	Fluctuating velocity (m/s)
u_{avg}	Mean flow velocity (m/s)
w_t	Dry matter at any time moment t (kg)
w_d	Dry matter (kg)
y^+	Dimensionless normal distance from the wall

Greek symbols

ρ	Drying air density (kg/m^3)
μ	Viscosity (N$\cdot$s/m^2)
Δp_{tot}	Total pressure drop (Pa)
Δp	Pressure drop in the dryer (Pa)
ζ_{tot}	Total loss coefficient based on drying chamber dynamic pressure
α	Permeability of the tray (m^2)
Δm	Thickness of the medium (m)

Subscripts

i	Index of Cartesian components
D_h	Hydraulic diameter

ACKNOWLEDGMENTS

REFERENCES

[1] C. T. Kiranoudis, V. T. Karathanos and N. C. Markatos, "Computational fluid dynamics of industrial batch type dryers of fruits", Drying Technology, Vol. 17, pp. 1-25, 1999.

[2] F. Roman, V. Stahl-Schafer and O. Hensel, "Improvement of air distribution in a fixed-bed dryer using computational fluid dynamics", Biosystems Engineering, Vol 112, pp. 542-550, 2012.

[3] D. P. Margaris and A. G. Ghiaus, "Dried product quality improvement by air flow manipulation in tray dryers", Journal of Food Engineering, Vol. 75, pp. 542-550, 2006.

[4] Y.Amanlou, and A. Zomordian, "Applying CFD for designing a new fruit cabinet dryer", Journal of Food Engineering, Vol. 101, pp. 8-15, 2010.

[5] E. Mathioulakis, V. T.Karathanos, and V. G. Belessiotis,"Simulation of air movement in a dryer by computational fluid dynamics: Application for the drying if fruits", Journal of Food Engineering, Vol. 36, pp. 183-200, 1998.

[6] T. Norton and D. W. Sun, "Computational fluid dynamics (CFD) – an effective and efficient design and analysis tool for the food industry: a review", Trends in Food Science and Technology, Vol. 17, pp. 600-620, 2006.

[7] D. S. Miller, "Internal flow systems", BHRA Fluid Engineering, Vol. 5, 1978.

[8] R. D. Mehta and P. Bradshaw, "Design rules for small low speed wind tunnels", Aeron. Journal, 1979.

[9] P. Bradshaw and R. C. Pankhurst, "The design of low speed wind tunnels", Prog. Aeron. Sci., Vol. 5, 1964.

[10] A. Pope and J. J. Harper, "Low speed wind tunnel testing", J. Wiley and Sons, 1966.

[11] B. Eckert , F. Pfluger , "The resistance coefficient of commercial round wire grids", NACA TM 1003, 1942.

[12] K. E. G. Wieghardt, "On the resistance of screens", Aeron. Quartley, Vol. 4, 1953.

[13] I. E. Idelchik, "Handbook of hydraulic resistance", 3rd ed., CRC Press Inc, 1994.

[14] J. Tu , G.H. Yeoh and C.Liu, "Computational Fluid Dynamics. A Practical Approach", 1st ed., Butterworth-Heinemann, 2008.

[15] Fluent 6.3 User's Guide, Fluent Inc., 2006.

[16] AOAC, Official Methods of Analysis, 15th Ed., Association of Official Analytical Chemists: Arlington,VA, 1990.

[17] T.Madhiyanon, A. Phila and S. Soponronnarit, "Models of fluidized bed drying for thin-layer chopped coconut", Applied Thermal Engineering, 29, p.p. 2849-2584, 2009.

[18] R. Lopez, A. de Ita and M. Vaca, "Drying of prickly pear cactus cladodes (Opuntia ficus indica) in a forced convection tunnel", Energy Conversion and Management, 50, p.p. 2119-2126, 2009.

[19] G. Page, "Factor influencing the maximum rates of air drying shelled corn in thin layer", Master Thesis, Purdue University, 1949.

[20] D. Tzempelikos, A. Bardakas, A. Vouros, D. Tsepenekas, A. Filios and D. Margaris, "An experimental study on convective drying of quince", EENVIRO Conference, 19 – 20 September, Bucharest, Romania, 2013.

[21] K. Sacilik & A. K. Elicin, "The thin layer drying characteristics of organic apple slices", Journal of Food Engineering, 73, p.p. 281-289, 2006.

[22] I. Doymaz, "An Experimental Study on Drying of Green Apples", Drying Technology, 27, p.p. 478-485, 2009.

[23] M. K. Krokida, V. T. Karathanos, Z. B. Maroulis & D. Marinos-Kouris, "Drying Kinetics of some vegetables", Journal of Food Engineering, 59, p.p. 391-403, 2003.

[24] V. T. Karathanos & V. G. Belessiotis, "Application of a thin-layer equation to drying data of fresh and semi-dried fruits", Journal of Agricultural Engineering Research, 74, p.p. 355-361, 1999.

[25] A. Kaya, O. Aydin, C. Demirtas & M. Akgun, "An experimental study on the drying kinetics of quince", Desalination, 212, p.p. 328-343, 2007.

[26] S. J. Babalis & V. G. Belessiotis, "Influence of the drying conditions on the drying constants and moisture diffusivity during the thin-layer drying of figs", Journal of Food Engineering, 65, p.p. 449-458, 2004.

[27] M. Aghbashlo, M. H. Kianmehr & A. Arabhosseini, "Modeling of thin-layer drying of potato slices in length of continuous band dryer", Energy Conversion and Management, 50, p.p. 1348-1355, 2009.